

Calibration and Evaluation of a Motion Measurement System for PET Imaging Studies

Junxiang Wang¹, Ti Wu², Iulian Iordachita¹, Peter Kazanzides²

¹*Dept. of Mechanical Engineering, Johns Hopkins University, Baltimore, MD 21218, USA*
Email: [jwang334, iordachita]@jhu.edu

²*Dept. of Computer Science, Johns Hopkins University, Baltimore, MD 21218, USA*
Email: pkaz@jhu.edu

Positron Emission Tomography (PET) enables functional imaging of deep brain structures, but the bulk and weight of current systems preclude their use during many natural human activities, such as locomotion. The proposed long-term solution is to construct a robotic system that can support an imaging system surrounding the subject's head, and then move the system to accommodate natural motion. This requires a system to measure the motion of the head with respect to the imaging ring, for use by both the robotic system and the image reconstruction software. We report here the design, calibration, and experimental evaluation of a parallel string encoder mechanism for sensing this motion. Our results indicate that with kinematic calibration, the measurement system can achieve accuracy within 0.5 mm, especially for small motions.

Keywords: position sensing; string encoders; parallel mechanism; kinematic calibration; robotic imaging

1. Introduction

Positron Emission Tomography (PET) relies on the injection of a radioactive tracer, which is then preferentially absorbed by specific tissues (based on the choice of tracer). The absorbed tracer emits positrons that react with nearby electrons, creating a pair of annihilation (gamma) photons that travel in opposite directions and are detected by the PET imaging ring. Higher sensitivity can be achieved by placing the PET detectors as close as possible to the subject. To accomplish brain imaging during locomotion and other natural activities, a wearable imaging device, such as the Helmet PET [1], would be the ideal approach. Under current technology, however, sufficient sensitivity for neuroscience research would require a PET detector weighing 10 kg or more [2] (other estimates are 15-20 kg). Therefore, we are alternatively exploring the possibility of active compensation for head motion, where the PET imaging ring is suspended over the subject's head by a robotic system while the subject walks on a treadmill or engages in similar activities, as illustrated in Fig. 1. The robotic system is tasked with keeping the imaging ring approximately centered around the subject's head (coarse motion compensation), while the image reconstruction algorithm corrects residual motion (fine motion compensation). This is an example of human-robot interaction, where the robot must safely move in proximity of the human.

Given the high safety requirement when moving a 15-20 kg weight over a human head with a robot, we plan to utilize both mechanical and optical measurement systems, and possibly also inertial sensing, to attain redundant sensing of the relative motion between the subject's head and the PET imaging ring. This paper addresses the design, calibration, and evaluation of a mechanical sensing system, consisting of six string encoders connecting the PET detector to a safety helmet attached to the subject's head. This system will provide the primary measurement for controlling the robot (coarse motion compensation) according to our current plan, due to its robustness and high-frequency measurements (on the order of 1 kHz). On the contrary, optical sensing can achieve high accuracy, but at a cost of lower-frequency feedback (on the order of 30-60 Hz) and risk of failing to provide a measurement. The decision on which measurement system is used for the purpose of image reconstruction (fine motion compensation) has not been made, as it involves evaluating the accuracy of the measurement systems and meeting the requirement for the reconstruction process. According to the imaging scientists, motion measurements for this task should be accurate to within about 0.5 mm. Since the maximum radius of a human head is about 100 mm [3], the accuracy requirement ϵ (mm) can be expressed as:

$$\epsilon = \Delta t + 100 \tan(\Delta\theta) \leq 0.5 \quad (1)$$

where Δt is the translation error (mm) and $\Delta\theta$ is the rotation error. In practice, this requirement will be stricter than necessary, since targets of interest will likely be closer to the center of the head than the above assumed 100 mm. Nevertheless, evaluating the mechanical sensing system against this requirement is one of the goals of this paper.

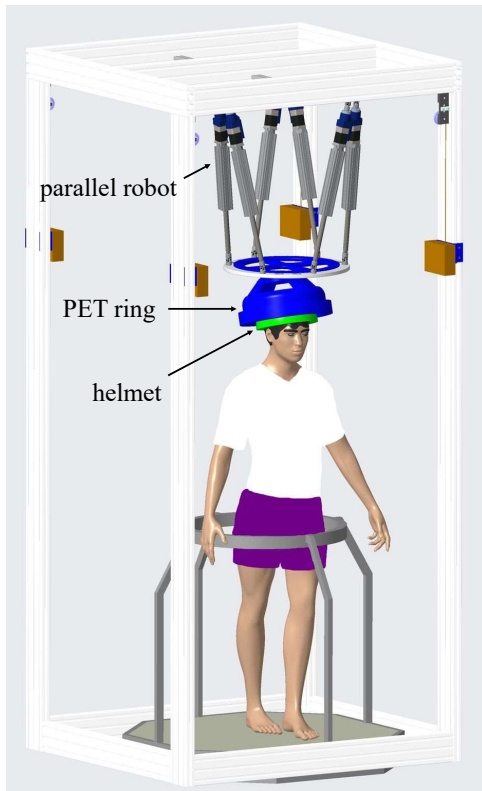


Fig. 1. System concept: Parallel robot supports PET imaging ring around a subject’s head, while the subject walks on a treadmill. The string encoder system measures the position of a helmet (green), worn by the subject, with respect to the imaging ring (blue).

Motion correction is also relevant for conventional PET imaging, and several researchers have investigated different approaches for sensing this motion. Especially, different markerless approaches have been studied extensively in recent years. Olesen [4,5] describes a system that incorporates a near infrared light emitting diode into a digital light processing projector to result in a surface scanner, tracking the head motion by creating a 3D point cloud on the head surface. This system is mounted directly on the PET imaging device, and while providing high accuracy of less than 0.3 mm, adds considerable weight to the imaging ring. This setup also requires clearance between the patient’s head and the imaging ring for the emission and processing of the near infrared light, which conflicts with our desire for a compact, highly-sensitive imaging system. Other methods rely more on image processing, thus reducing the required amount of computation compared to such a 3D surface

imaging system. Kyme [6] and Anishchenko [7] utilized four cameras to record the patient’s head, followed by detection of facial features from the video and determination of the 6 degree-of-freedom (DOF) movement of the head. However, this markerless approach could only achieve an accuracy of about 2 mm.

Chamberland [8] uses positron emission fiducial markers to detect tumor movement for more accurate targeting in radiotherapy. This approach benefits from having motion be directly measurable in the images, which is ideal for the fine motion correction, but is not fast enough to control the robot for the coarse motion correction. Moreover, the fiducial marker would be visible in the reconstructed image and could interfere with perception of nearby brain structures.

We previously determined the typical range of head motion, as well as velocity and acceleration, by analyzing motion capture and accelerometer data from subjects during overground and treadmill walking, respectively [9]. We evaluated the ability of a simulated robot to compensate for the recorded head motion, without collision between a helmet of dimension 263 mm x 215 mm and an imaging ring 300 mm in diameter. Our results support the feasibility of such a compensation, given a robot capable of tracking typical head motions within about 100 ms. This assertion will be experimentally verifiable with the measurement system that is the focus of this work. Section 2 presents the measurement system design, implementation, and calibration; Section 3 explains our means of evaluating the measurement system, including integration of a robot for providing ground-truth displacements. This is followed by calibration and accuracy results in Section 4, and conclusions in Section 5. The design of the measurement system and a preliminary accuracy evaluation (considering only translation measurement error under single-axis displacements) were reported in [10]; this paper adds the kinematic calibration method (see Section 2.3) and a more extensive accuracy evaluation, including translation and rotation errors under multi-axis displacements.

2. System

This section describes the design and construction of our mechanical measurement system using parallel string encoders, followed by a kinematic analysis and homing procedure (to determine initial string lengths). Then we discuss how the encoder attachment points and string lengths are adjusted using kinematic calibration.

2.1. Mechanical design

We designed a parallel structure (essentially a passive parallel robot) consisting of 6 string encoders attached between the helmet worn by the subject and the imaging ring. For this system, forward kinematics converts the measured joint positions (string encoder lengths) to Cartesian pose. Since at least 6 string encoders are needed to provide 6 DOF, multiple configurations are possible. A Stewart platform structure

was selected over other common cable-driven parallel robots (CDPRs) [11] and parallel measuring structures [12] due to its compactness and prevalence [13], as well as its resistance against string interference (i.e., the strings should not come into contact with each other, the helmet, or the imaging device).

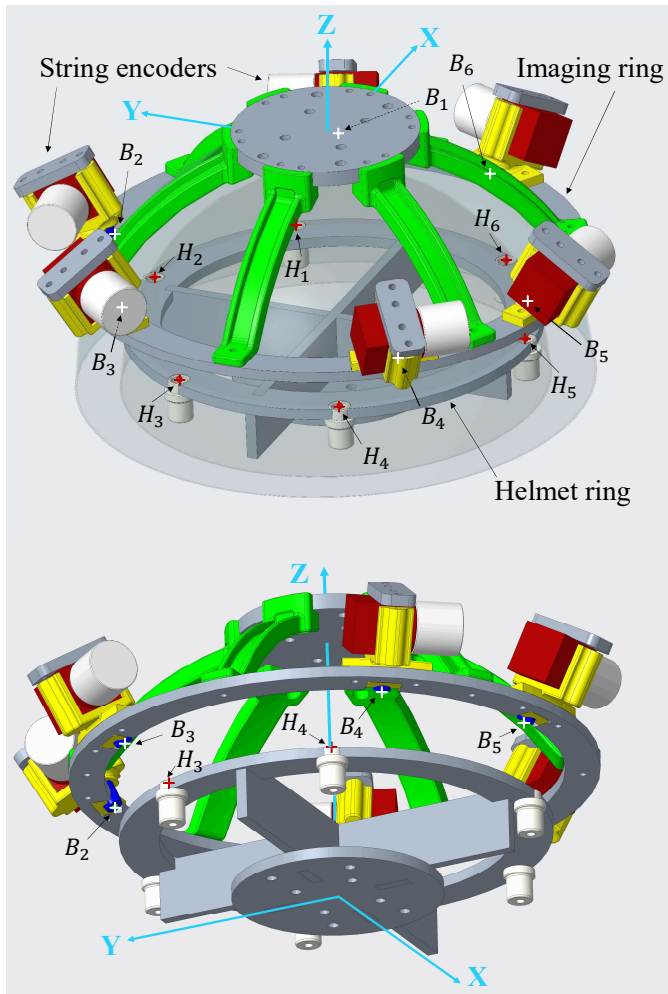


Fig. 2. CAD model of string encoder system, with base (imaging ring) and helmet attachment points labeled

Various Stewart platform designs were considered, evaluated based on motion sensitivity (resolution) and isotropic performance. The current design relies upon the approximation of the imaging ring as a sphere of 300 mm diameter and the helmet/head as a sphere of 250 mm diameter. This approximation serves only for initial evaluation purposes, as the PET detector is expected to be cylindrical instead of spherical, and the helmet is expected to be elliptical with a major axis of about 263 mm instead of circular. The prototype comprises two attachment rings—one represents the imaging ring, and the other represents the helmet. The placement of the rings within the respective spheres leads to the imaging ring having a diameter of 261.32 mm and

the helmet ring a diameter of 235.42 mm. Fig. 2 depicts the string encoder system in two views of a CAD model generated with Creo. The locations of every pair of string attachment points are labeled in the top view angle, while a more direct view at the attachment points on the imaging ring is provided on the bottom. The orientation of the system is also shown in the figure: in the nominal configuration, the helmet sphere is concentric with the base (PET imaging ring) sphere, and the coordinate axes of the spheres are aligned as well. The designed string attachment points are given in Table 1, where B_i and H_i ($i = 1 \dots 6$) are the base and helmet attachment points, respectively.

Table 1. Designed Stewart platform attachment point coordinates (units: mm)

Encoder Number	B_i			H_i		
	X	Y	Z	X	Y	Z
1	121.39	48.35	73.67	96.99	66.70	42.06
2	-18.82	129.30	73.67	9.27	117.35	42.06
3	-102.56	80.95	73.67	-106.26	50.64	42.06
4	-102.56	-80.95	73.67	-106.26	-50.64	42.06
5	-18.82	-129.30	73.67	9.27	-117.35	42.06
6	121.39	-48.35	73.67	96.99	-66.70	42.06

2.1.1. Construction

Each of the six string encoders (MPS-XXXS-200MM-P, Miran Industries, China) has a 200 mm measuring range at 60 counts/mm resolution. The string encoder bodies are secured onto the PET imaging ring and the mobile ends onto the helmet. The custom portions of the system comprise laser-cut acrylic plates and 3D-printed (Stratasys F170) ABS components. The geometry of the attachment rings and string connection points follows the Stewart platform presented above.

The string encoders are incremental, with quadrature outputs (A and B channels) and an index pulse (I channel). A custom board was created to interface these signals to an FPGA board developed for the da Vinci Research Kit (dVRK) [14]. The FPGA firmware already included a four-channel encoder interface module, with modification applied to support a maximum of eight channels. The software for testing is implemented on a PC, which is connected to the FPGA board via a UDP socket.

2.2. String encoder kinematics

The string encoder system adopts a Stewart platform structure; hence the standard kinematics model is applied, in which the inverse kinematics (from Cartesian pose to string lengths) is easily computed knowing the string attachment points on the base (PET imaging ring) and the moving platform (helmet). Let X denote the Cartesian pose (transform) of the helmet with respect to the base, and B_i and H_i

($i = 1 \dots 6$) denote the coordinates of the base and helmet attachment points, respectively. Then the computed string lengths, \hat{L}_i , are solved from the following inverse kinematics equation:

$$\hat{L}_i = \|X * H_i - B_i\| \quad (2)$$

The forward kinematics involves higher complexity and requires numerical computation, as described in [15]. Let L_i denote the measured string lengths. Then the estimated Cartesian pose of the helmet with respect to the base, \hat{X} , is obtained from the following iterative computation:

$$\hat{X}_{k+1} = \hat{X}_k + J(\hat{L}_k) (L_m - \hat{L}_k) \quad (3)$$

where k is the iteration counter, $J(\hat{L}_k)$ is the Jacobian and \hat{L}_k is the inverse kinematics solution, eq. (2), corresponding to \hat{X}_k . The Cartesian pose here is a six-dimensional vector with the rotation component represented in Euler angles, following the intrinsic ZYX convention, i.e., with respect to the helmet coordinate system shown in Fig 2. Subsequently in this paper, the rotation angle about the z-axis is referred to as roll, the angle about the y-axis as pitch, and the angle about the x-axis as yaw. The forward kinematics iteration is terminated when the combined error in string length, computed with $\|L_m - \hat{L}_k\|$, is below a specified threshold (0.01 mm in our implementation), hence signalling convergence. The second condition for termination is the iteration counter reaching a specified limit (50 in our implementation). Convergence is generally observed in three to four iterations. We would like to point out that for a parallel structure, the more practical approach to obtain the Jacobian is to compute the inverse Jacobian and then numerically solve for its pseudo-inverse.

2.2.1. Homing procedure

Since the string encoders only measure relative displacements, a homing procedure is required to set a reference absolute displacement, accomplished by utilizing the encoder index pulses transmitted on a separate channel from the regular quadrature signals. Through each encoder's 200 mm range of travel, three index pulses are produced, evenly spaced apart by 4000 counts (one-third of the total measurement range). Each string encoder possesses a different position of the first index pulse, and the absolute displacements corresponding to these positions were recorded before the string encoders were installed.

Based on this information, whenever the homing procedure needs to be performed, the first index pulse can be triggered by bringing the measuring ends as close to the encoder bodies as possible and subsequently captured by the FPGA firmware. Next, with calculation of the difference between these measured values and the recorded positions, offsets can be set in order to convert the relative displacements to absolute displacements.

2.3. Kinematic calibration

2.3.1. Attachment point and string length adjustments

The string encoder attachment points are influenced by several factors that lead to slight deviations from the kinematic model presented in Table 1. First of all, due to manufacturing inaccuracy, the real attachment points unavoidably differ from the exact values listed in Table 1, and hence are in need of adjustment. On the other hand, we also performed an adjustment for the measured string lengths due to an observed measurement deficit. As depicted in Fig. 3, the encoder has a circular guide channel for the string, and the center of that channel is the designed attachment point on the base, but the string instead lies against the edge of the channel in reality. This shift might be accounted for by adjusting the attachment point coordinates, along with the tuning needed due to manufacturing inaccuracy. However, during the helmet platform's motion, the string's position within the channel is also frequently shifted, especially when the motion is around the nominal position. This would hence require update of the attachment point coordinates during operation, complicating the approach. Instead, it was observed that because the guide channels are oriented at an angle, each string consistently remains in contact with the edge of the channel for a small range of motion around the nominal position. Thus, the actual reading reported by each encoder is less than the designed situation where the string exits from the center of the guide channel, and this difference always remains constant. Consequently, from kinematic calibration, we would like to determine for each string encoder this string length offset ΔL_i , as well as updated coordinates for B_i and H_i that reflect manufacturing deviation from the designed values, hence a total of seven parameters.

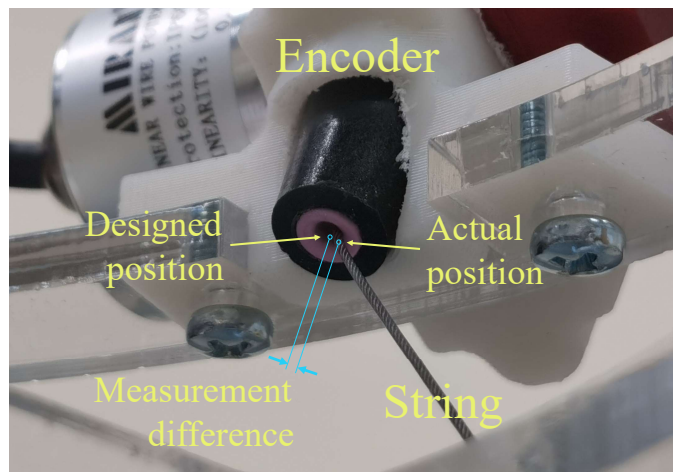


Fig. 3. Deviation of the encoder string from the hole center

2.3.2. Parameter optimization

As described in Section 2.2, the forward kinematics for the Stewart platform possesses only a numerical solution, whereas the inverse kinematics has an analytical solution. Since the parameter optimization relies on taking derivatives, we chose to perform the minimization based on the inverse kinematics formulation, similar to approaches taken by other researchers [16–18], by minimizing the string length measurement error in the Stewart platform’s joint space. Moreover, performing calibration in inverse kinematics also provides the advantage of being able to solve the parameters of each leg independently, because the inverse kinematics equation (2) is specific to each leg and only depends on the platform pose in addition to the kinematic parameters of that leg. The following introduces the cost function of the minimization problem involved in the kinematic calibration, as well as the process of solving it using the Gauss-Newton algorithm.

First, denote the collection of the seven parameters mentioned in Section 2.3.1 as a vector:

$$\boldsymbol{\theta}_i = \begin{bmatrix} B_i \\ H_i \\ \Delta L_i \end{bmatrix}$$

Next, suppose we have a ground-truth measurement of the Cartesian pose of the helmet with respect to the base, denoted as X . Then, the ground-truth string length is given by the inverse kinematics equation (2) and consequently, if we denote the measured string length as L_i , then the error of this measurement is represented by the function:

$$f_i(\boldsymbol{\theta}_i) = L_i + \Delta L_i - \|X * H_i - B_i\| \quad (4)$$

where $i = 1 \dots 6$ is the encoder index. If the helmet is moved to n different poses, then for each encoder we have n functions representing the measurement error. With $j = 1 \dots n$ as the pose index:

$$f_{i,j}(\boldsymbol{\theta}_i) = L_{i,j} + \Delta L_i - \|X_j * H_i - B_i\| \quad (5)$$

Now, we are able to apply the Gauss-Newton algorithm to minimize the sum of squares of these n functions for each encoder independently, that is, solve 6 minimization problems with the cost functions defined as:

$$C_i(\boldsymbol{\theta}_i) = \sum_{j=1}^n f_{i,j}(\boldsymbol{\theta}_i)^2 \quad (6)$$

The algorithm proceeds by first determining the Jacobian of the vector-valued function

$$\mathbf{f}_i(\boldsymbol{\theta}_i) = \begin{bmatrix} f_{i,1}(\boldsymbol{\theta}_i) \\ \vdots \\ f_{i,n}(\boldsymbol{\theta}_i) \end{bmatrix}$$

If R_j represents the rotation component of pose X_j , the

Jacobian is given by:

$$\mathbf{J}_{\mathbf{f}_i}(\boldsymbol{\theta}_i) = \begin{bmatrix} \frac{(X_1 * H_i - B_i)^\top}{\|X_1 * H_i - B_i\|} - \frac{(X_1 * H_i - B_i)^\top R_1}{\|X_1 * H_i - B_i\|} & 1 \\ \vdots & \vdots \\ \frac{(X_n * H_i - B_i)^\top}{\|X_n * H_i - B_i\|} - \frac{(X_n * H_i - B_i)^\top R_n}{\|X_n * H_i - B_i\|} & 1 \end{bmatrix} \quad (7)$$

Next, the Gauss-Newton algorithm states that the parameter update between iteration step s and step $s + 1$

$$d\boldsymbol{\theta}_i = \boldsymbol{\theta}_i^{(s+1)} - \boldsymbol{\theta}_i^{(s)}$$

is obtained as the solution to the following linear system:

$$\mathbf{J}_{\mathbf{f}_i}(\boldsymbol{\theta}_i^{(s)})^\top \mathbf{J}_{\mathbf{f}_i}(\boldsymbol{\theta}_i^{(s)}) d\boldsymbol{\theta}_i = -\mathbf{J}_{\mathbf{f}_i}(\boldsymbol{\theta}_i^{(s)})^\top \mathbf{f}_i(\boldsymbol{\theta}_i^{(s)}) \quad (8)$$

Starting from the initial guess of $\boldsymbol{\theta}_i^{(0)}$ with coordinates from Table 1 and $\Delta L_i = 0$, the iteration is repeated until the cost function between the previous and current sets of parameters changes by less than 0.01%. The same collection of poses is used to calibrate parameters for all encoders. Details for obtaining the ground-truth poses are presented in the following section.

3. Experiments

This section presents our experimental setup that provides a ground-truth reference for the string encoder system using a robot, followed by the data collection process for kinematic calibration, as well as computation of measurement errors in accuracy evaluation.

3.1. Experimental setup

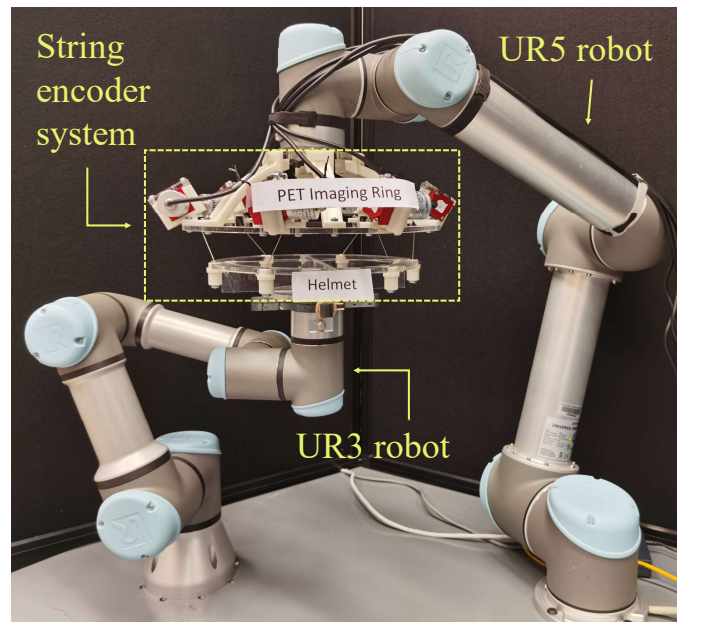


Fig. 4. Experimental setup consisting of string encoder system and UR3 and UR5 robots

To analyze the relative motion between the helmet (head) and the PET imaging system, in addition to the string encoder system described in Section 2, we employed an experimental setup consisting of a UR3 robot (Universal Robots, Odense, Denmark) to provide helmet ring movement and a UR5 robot for supporting the PET imaging ring, as shown in Fig. 4. In the experiments reported in this paper, the UR5 robot was not moved, whereas in future proof-of-concept work, its commanded motion will attempt to keep the (mock) PET imaging ring centered over the helmet based on the measured head position. In the longer term, the UR5 payload is insufficient to support the weight of an actual PET system and consequently a custom parallel robot, similar to the one shown in Fig. 1, will be designed and will replace the UR5.

Because the goal of the UR3 robot is to provide precise helmet motions, the measurement accuracy of the robot was first verified against a dial indicator (543-693B, Mitutoyo Corp., Japan), for a ± 10 mm range of motion. The robot motion is limited to this particular region since, as mentioned in Section 2.1, the designed clearance between the helmet and the PET detector is only about 15 mm. Since the UR3 end-effector is cylindrical, a part was designed and 3D-printed to provide a flat edge for ease of measurement. We interfaced to the UR3 robot via TCP, using its real-time script interface.

Our previous work [10] includes a figure illustrating this dial indicator setup, as well as the full result of the accuracy verification. We found that the difference between the commanded displacement to the robot and the measured displacement from the dial indicator generally stays less than 0.1 mm, and the rough surface on the 3D-printed part could have partially contributed to this discrepancy. Nonetheless, it can be concluded that the accuracy of the UR3 robot is around 0.1 mm and thus suffices to provide ground-truth helmet motions in the experiments conducted.

3.2. Transformation between robot and string encoder system

Our calibration procedure requires ground-truth pose information, which can be provided by the UR3 robot if its coordinate system is registered to the string encoder coordinate system. We accomplished this by considering that the transformation between the PET imaging ring (base) and the robot, ${}^B E_R$, is fixed because the UR5 robot remains stationary. After setting the robot tool center point (TCP) coincident with the center of the helmet, the measured pose outputted from the robot interface corresponds to the transformation between the robot and the helmet, ${}^H E_R$. Then, ${}^B E_R ({}^H E_R)^{-1} = {}^B E_H$, which is the transformation between the PET imaging ring and the helmet ring and the same transformation measured by the string encoder system. Since under the nominal position between the base and the helmet, this transformation is simply the identity, the UR3 robot only needs to query ${}^H E_R$ once at the nominal position to store it as ${}^B E_R$. Afterwards, the measurements from the

UR3 robot can be converted to a 6 DOF pose in the string encoder coordinate system by computing ${}^B E_R ({}^H E_R)^{-1}$ as a transformation and extracting the translation and rotation components. For clarity and convenience, we denote this platform pose computed from robot measurements as X^r , and the platform pose computed with forward kinematics of the string encoder system as X^e .

3.3. Calibration procedure

The kinematic calibration is performed by moving the UR3 robot to various points within the workspace around the nominal position, recording the string lengths $L_{i,j}$, and using the robot-reported platform poses X_j^r as the ground-truth poses in eq. (7) to solve the minimization problem. The waypoints selected are all the points within a 15 mm radius from the nominal position, with one at the center, and the rest equally spaced 5 mm apart. The first set is collected with the rotation being the identity, and afterwards, the same waypoints are traversed five more times, each time with a different rotation, where each Euler angle is randomly sampled from a Normal distribution with zero mean and standard deviation of three degrees. This sums to an overall collection of 732 points, and as mentioned in Section 2.3, this same collection can be used to calibrate the parameters for each leg independently. Since the linear system in eq. (8) has more equations than unknowns, a least-squares solution is used to find the parameter update between iteration steps.

3.4. String encoder measurement accuracy evaluation

To perform the accuracy evaluation, we first designed a set of points that evenly explore the workspace of the helmet—up to 10 mm or deg away from the nominal position. We accomplished this by forming 10 spherical shells, with the radii ranging from 1 to 10 in increments of 1. Each shell of radius r contains 14 points evenly spaced apart—six along the coordinate axes (i.e. $[r, 0, 0]$, $[0, r, 0]$, $[0, 0, r]$ and their negatives) and one in the middle of each octant, with each coordinate equal to $\pm\sqrt{r/3}$ (for example, the coordinates in the first octant are given by $[\sqrt{r/3}, \sqrt{r/3}, \sqrt{r/3}]$). Summing the points in all ten shells results in a total of 140 points in \mathbb{R}^3 . Interpreting these 140 points as Cartesian positions with mm as the unit yields the accuracy test set for translational motion. On the other hand, interpreting the same set in \mathbb{R}^3 as Euler ZYX rotation angles in degrees yields the test set for rotational motion. The robot was commanded to first execute purely translational motion, followed by purely rotational motion, with the test sets described above, in order to provide more information about the difference in accuracies associated with the two different types of motion. At each pose, the string lengths were recorded, adjusted by the offsets identified from kinematic calibration, and then the forward kinematics was applied under the calibrated at-

tachment point coordinates, obtaining the 6 DOF Cartesian pose.

The computed pose is denoted by $X^e = (t^e, R^e)$, where t^e is the translational component and R^e the rotational component, and similarly the ground-truth pose is $X^r = (t^r, R^r)$. The translation error of the string encoder system’s measurement is

$$\Delta t = \|t^e\| - \|t^r\| \quad (9)$$

and the rotation error is

$$\Delta \theta = \|(\ln R^e)^\vee\| - \|(\ln R^r)^\vee\| \quad (10)$$

where the “vee” operator $^\vee$ denotes the conversion from a skew-symmetric matrix to the corresponding vector, and hence the rotation error represents the difference in the *angle* value of the axis-angle representations of the measured and ground-truth rotations. Analogously, the translation error represents the difference in magnitudes between the measured and ground-truth translations, thus eliminating potential error caused by coordinate system registration. The accuracy of the string encoder measurement system is evaluated by calculating both the translation error and the rotation error at each position of the UR3. Moreover, for clarity, we use the subscript “T” to denote when the UR3 is performing a purely translational motion, and the subscript “R” for a purely rotational motion. For example, Δt_R represents the translation measurement error when the UR3 is performing rotational motion only. We also compute the combined error, ϵ , using equation (1).

4. Results

4.1. Calibration results

The kinematic calibration is carried out as mentioned previously, with the data collection process described in Section 3.3 and the optimization described in Section 2.3.2. The optimization algorithm converges rapidly and meets the 0.01% threshold after three to four iterations for all encoders.

Table 2 shows the updated system parameters after calibration, including the base attachment point coordinates B_i , the helmet attachment points H_i , as well as the string length offset dL_i for each encoder (hence each leg of the Stewart platform).

Table 2. Calibrated Stewart platform kinematic parameters—attachment point coordinates and string length offsets (units: mm)

Encoder Number	B_i			H_i			dL_i
	X	Y	Z	X	Y	Z	
1	115.48	47.31	71.31	92.11	63.65	41.78	1.49
2	-16.43	128.18	70.46	9.31	114.63	42.16	0.65
3	-100.45	79.93	70.69	-103.85	48.06	41.49	5.43
4	-100.82	-76.10	71.96	-103.35	-48.84	43.14	4.05
5	-19.56	-124.92	72.31	8.59	-114.24	42.30	5.63
6	117.71	-46.15	75.75	94.38	-64.85	45.04	4.33

The dL_i values are all positive, suggesting that the raw measurements are short of the ideal measurements, which matches with the predicted measurement deficit as explained in Section 2.3.1. Furthermore, the attachment point coordinates between Tables 1 and 2 each differ by less than 5 mm, which is a reasonable representation of the potential errors in manufacturing and installation. The updated set of parameters is then used in the subsequent accuracy evaluation.

4.2. String encoder system accuracy evaluation

The accuracy evaluation was performed as described in Section 3.4. Table 3 shows the translation and rotation measurement errors when the ground-truth motion is translation only, accompanied by comparison between calibrated and uncalibrated kinematic parameters. Table 4 shows the case with purely rotational ground-truth motion, and the data for both tables are represented in Fig. 5.

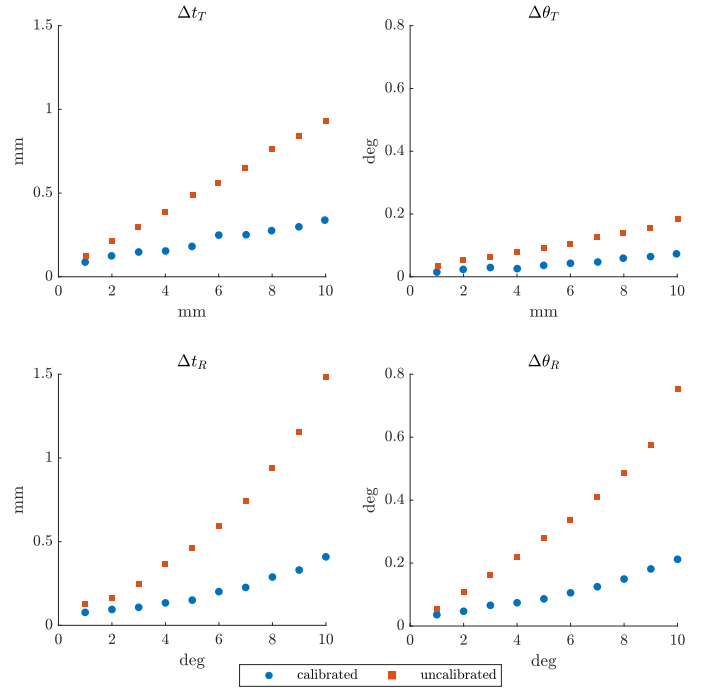


Fig. 5. Accuracy evaluation result of the string encoder system, with comparison before and after calibration. Vertical axes represent translation error, Δt (mm), and rotation error, $\Delta \theta$ (deg). Horizontal axes represent corresponding displacements (mm or deg).

The results indicate that kinematic calibration reduced the overall RMS errors by 60-70%. With the calibrated parameters, we have achieved translation RMS errors less than 0.3 mm as well as rotation RMS errors less than 0.2 deg for all motions, with more error associated with rotational

motion than translational motion. The results also show that the combined error, ϵ , is less than the 0.5 mm threshold for translations up to 10 mm and rotations up to 7 deg. This indicates that the string encoder measurement system can meet the requirement for fine motion correction (during image reconstruction) assuming that the coarse motion correction (due to the robot moving the imaging ring) can keep the imaging ring within these translation and rotation limits. Further testing is required to determine whether these limits would need to be reduced to handle motions that include both translation and rotation. In addition, the current accuracy evaluation was performed under static conditions, and the error would likely be higher under dynamic conditions.

Table 3. RMS translation error, Δt (mm), and rotation error, $\Delta\theta$ (deg), due to translational displacements (in mm) from the origin, with uncalibrated and calibrated parameters. ϵ is the combined error, eq. (1).

Displ. (mm)	Uncalibrated			Calibrated		
	Δt_T	$\Delta\theta_T$	ϵ_T	Δt_T	$\Delta\theta_T$	ϵ_T
1	0.12	0.04	0.18	0.09	0.01	0.11
2	0.22	0.05	0.31	0.12	0.02	0.17
3	0.30	0.06	0.41	0.15	0.03	0.20
4	0.39	0.08	0.52	0.15	0.03	0.20
5	0.49	0.09	0.65	0.18	0.04	0.24
6	0.56	0.11	0.75	0.25	0.04	0.32
7	0.65	0.13	0.87	0.25	0.05	0.33
8	0.76	0.14	1.00	0.28	0.06	0.38
9	0.84	0.16	1.11	0.30	0.06	0.41
10	0.93	0.18	1.25	0.34	0.07	0.47
Overall RMS	0.59	0.11	0.78	0.22	0.05	0.30

5. Conclusions

We developed a mechanical 6 DOF measurement system comprising six parallel string encoders, configured as a Stewart platform structure. The designed task of this system is to provide measurement of the motion of a helmet, worn by a human subject, relative to a PET imaging device supported by a robotic system. We performed kinematic calibration to improve the measurement accuracy of the system and conducted experiments with a robot providing precise helmet motions. The results indicate that the measurement accuracy can meet the 0.5 mm requirement for fine motion correction during image reconstruction, assuming that the robotic system can keep the PET imaging ring “near” the nominal (center) position. Based on our current results, “near” is defined as within 10 mm and 7 deg, but this definition may be changed in the future as more complex motions are evaluated under dynamic conditions.

Table 4. RMS translation error, Δt (mm), and rotation error, $\Delta\theta$ (deg), due to rotational displacements (in deg) from the origin, with uncalibrated and calibrated parameters. ϵ is the combined error, eq. (1).

Displ. (deg)	Uncalibrated			Calibrated		
	Δt_R	$\Delta\theta_R$	ϵ_R	Δt_R	$\Delta\theta_R$	ϵ_R
1	0.13	0.05	0.22	0.08	0.04	0.14
2	0.17	0.11	0.36	0.09	0.05	0.18
3	0.25	0.16	0.53	0.11	0.07	0.22
4	0.37	0.22	0.75	0.13	0.07	0.26
5	0.46	0.28	0.95	0.15	0.09	0.30
6	0.59	0.34	1.18	0.20	0.11	0.39
7	0.74	0.41	1.46	0.23	0.12	0.44
8	0.94	0.49	1.79	0.29	0.15	0.55
9	1.16	0.58	2.16	0.33	0.18	0.65
10	1.49	0.75	2.80	0.41	0.21	0.78
Overall RMS	0.76	0.40	1.45	0.23	0.12	0.44

Our next stage of development will involve emulation of realistic human head motion with the UR3 robot, using the previously recorded motion data that our prior work analyzed [9]. As the string encoder system collects measurement during the UR3 motion, we hope to have the UR5 robot and the PET imaging ring execute synchronized motion with the UR3 based on string encoder measurements. Eventually, since the UR5’s 5 kg payload falls short of the PET imaging ring mass of up to 20 kg, it would be replaced by a custom robot, but currently it serves as a prototype for proof-of-concept experiments and verification of our motion measurement and compensation system.

Acknowledgements

Stan Majewski initiated the investigation of robotic compensation for head motion during PET imaging. Yangzhe Liu participated in early design discussions of the measurement system.

References

- [1] S. Majewski, J. Proffitt, J. Breczynski-Lewis, A. Stolin, A. Weisenberger, W. Xi and R. Wojcik, HelmetPET: A silicon photomultiplier based wearable brain imager, *IEEE Nuclear Science Symposium and Medical Imaging Conference Record*, Valencia, Spain (Oct. 2011), pp. 4030–4034.
- [2] S. Majewski, The path to the “ideal” brain PET imager: The race is on, the role for TOF PET, *Il Nuovo Cimento C* **43**(1) (2020) 1–35.
- [3] Y. Rodrigues, Anthropometric analysis of human head for designing ballistic helmets, *Procedia Manufacturing* **3** (July 2015) 5475–5481.

- [4] O. V. Olesen, Markerless 3D head tracking for motion correction in high resolution PET brain imaging, PhD thesis, Technical University of Denmark (2011).
- [5] O. V. Olesen, J. M. Sullivan, T. Mulnix, R. R. Paulsen, L. Højgaard, B. Roed, R. E. Carson, E. D. Morris and R. Larsen, List-mode PET motion correction using markerless head tracking: Proof-of-concept with scans of human subject, *IEEE Transactions on Medical Imaging* **32**(2) (2013) 200–209.
- [6] A. Z. Kyme, S. Se, S. R. Meikle and R. R. Fulton, Markerless motion estimation for motion compensated clinical brain imaging, *Physics in Medicine & Biology* (2018).
- [7] S. Anishchenko, D. Beylin, A. Stepanov, I. Weinberg, S. Schaefer, V. Zavarzin, D. Shaposhnikov and M. Smith, Evaluation of a video-based head motion tracking system for dedicated brain PET, *Medical Imaging 2015: Physics of Medical Imaging* (2015).
- [8] M. Chamberland, R. Wassenaar, B. Spencer and T. Xu, Performance evaluation of real-time motion tracking using positron emission fiducial markers, *Medical Physics* **38**(2) (2011) 810–819.
- [9] Y. Liu, T. Wu, I. I. Iordachita, C. Paquette and P. Kazanzides, Analysis of human head motion and robotic compensation for PET imaging studies, *IEEE Engineering in Medicine & Biology Conf. (EMBC)*, (2021), pp. 4836–4839.
- [10] J. Wang, T. Wu, I. Iordachita and P. Kazanzides, Evaluation of a motion measurement system for PET imaging studies, *IEEE Intl. Symp. on Medical Robotics (ISMR)*, (Apr. 2022).
- [11] D. Lau, J. Eden, Y. Tan and D. Oetomo, CASPR: A comprehensive cable-robot analysis and simulation platform for the research of cable-driven parallel robots, *IEEE Intl. Conf. on Intelligent Robots and Systems (IROS)*, (Nov. 2016), pp. 3004–3011.
- [12] J. W. Jeong, S. H. Kim, Y. K. Kwak and C. C. Smith, Development of a parallel wire mechanism for measuring position and orientation of a robot end-effector, *Mechatronics* **8** (Dec. 1998) 845–861.
- [13] J.-P. Merlet, *Parallel Robots* (Springer, 2006).
- [14] P. Kazanzides, Z. Chen, A. Deguet, G. S. Fischer, R. H. Taylor and S. P. DiMaio, An open-source research kit for the da Vinci[®] surgical system, *IEEE Intl. Conf. on Robotics and Auto. (ICRA)*, Hong Kong, China (Jun 2014), pp. 6434–6439.
- [15] K. Harib and K. Srinivasan, Kinematic and dynamic analysis of Stewart platform-based machine tool structures, *Robotica* **21** (2003) 541–554.
- [16] H. Zhuang, O. Masory and J. Yan, Kinematic calibration of a Stewart platform using pose measurements obtained by a single theodolite, *IEEE/RSJ Intl. Conf. on Intelligent Robots and Systems (IROS)*, (1995), pp. 329–334.
- [17] H. Zhuang, J. Yan and O. Masory, Calibration of Stewart platforms and other parallel manipulators by minimizing inverse kinematic residuals, *Journal of Robotic Systems* **15**(7) (1998) 395–405.
- [18] R. Mayer and M. Oliviers, Global kinematic calibration of a Stewart platform, *ASME Dynamics System and Control Division*, **57** (01 1995).